

ARTICLE

Received 11 Jul 2014 | Accepted 28 Apr 2015 | Published 17 Jun 2015

DOI: 10.1038/ncomms8356

# Tissue landscape alters adjacent cell fates during *Drosophila* egg development

Lathiena A. Manning<sup>1</sup>, Ann Marie Weideman<sup>2</sup>, Bradford E. Peercy<sup>2</sup> & Michelle Starz-Gaiano<sup>1</sup>

Extracellular signalling molecules control many biological processes, but the influence of tissue architecture on the local concentrations of these factors is unclear. Here we examine this issue in the *Drosophila* egg chamber, where two anterior cells secrete Unpaired (Upd) to activate Signal transducer and activator of transcription (STAT) signalling in the epithelium. High STAT signalling promotes cell motility. Genetic analysis shows that all cells near the Upd source can respond. However, using upright imaging, we show surprising asymmetries in STAT activation patterns, suggesting that some cells experience different Upd levels than predicted by their location. We develop a three-dimensional mathematical model to characterize the spatio-temporal distribution of the activator. Simulations show that irregular tissue domains can produce asymmetric distributions of Upd, consistent with results *in vivo*. Mutant analysis substantiates this idea. We conclude that cellular landscape can heavily influence the effect of diffusible activators and should be more widely considered.

<sup>1</sup>Department of Biological Sciences, University of Maryland, Baltimore County (UMBC), 1000 Hilltop Circle, Baltimore, Maryland 21250, USA. <sup>2</sup>Department of Mathematics and Statistics, UMBC, 1000 Hilltop Circle, Baltimore, Maryland 21250, USA. Correspondence and requests for materials should be addressed to M.S.-G. (email: starz@umbc.edu)

During animal development, cells must respond to a changing environment and adopt proper identities. Diffusible, extracellular signals often instruct cells to take on particular fates. A classic type of instructive signal, called a morphogen, acts to pattern tissues in a concentration-dependent manner. While tissues are developing, a morphogen released from a defined region (source) creates a concentration gradient as the protein diffuses, and either interacts with a target cell or decays. In target cells, the morphogen level determines the appropriate response: concentrations above a certain threshold elicit one response, whereas those over another threshold prompt a different response. Thus, each cell receives positional information based on the gradient and this determines its fate (reviewed in refs 1–3). Our understanding of diffusible activators such as morphogens comes from a variety of contexts, but most studies presuppose that these signalling molecules act within a uniform landscape. During animal development, however, signalling occurs between cells that are packed into complex shapes. To understand how the intricate architecture of tissues can influence diffusible signals and pattern generation, we have focused on the egg development of *Drosophila melanogaster*.

The *Drosophila* egg chamber consists of germline and somatic cells, which are coordinated in their development. A single-layer epithelium of somatic follicle cells surrounds the oocyte and 15 large nurse cells that support egg growth<sup>4</sup>. Not all follicle cells are equivalent. Instead, multiple signalling pathways converge to define distinct subsets of cells (reviewed in refs 5–8). One early event is the specification of two pairs of specialized follicle cells, called polar cells, at the anterior and posterior poles of the epithelium. In mid-oogenesis, the two anterior polar cells secrete a ligand that specifies the nearest 6–8 follicle cells as a migratory cell type, the border cells<sup>9–14</sup>. Hours later, the border cells detach from the epithelium and migrate towards the oocyte, where they are required to make a viable egg, and remaining anterior follicle cells stretch over the nurse cells.

Anterior polar cells instruct neighbouring cell fates by activating the well-conserved Janus tyrosine kinase (JAK), and Signal transducer and activator of transcription (STAT) pathway (reviewed in refs 5,15–17). Polar cells secrete a diffusible signal, Unpaired (Upd), which acts as a morphogen. The Upd glycoprotein associates with heparin sulfate proteoglycans along follicle cells, which helps to establish its graded distribution as observed in fixed tissues<sup>14,18</sup>. Upd binds to a transmembrane receptor, Domeless (Dome), on neighbouring cells, thereby inducing JAK-mediated phosphorylation of associated STAT molecules<sup>5,9–11,16</sup>. Phospho-STAT dimers move to the nucleus and activate transcription. One direct STAT target gene is *slow border cells (slbo)*, which encodes a transcription factor required for border cell migration<sup>10–13</sup>. The gradient of Upd is reflected by the graded pattern of Slbo and STAT nuclear expression at the anterior pole; cells with the highest levels of these proteins become the motile border cells<sup>12,19</sup>. Although about 12 cells initially display STAT activation typically, only 6–8 maintain the above-threshold signalling needed for Slbo expression and border cell specification, whereas the other cells switch the signal off<sup>19,20</sup>. Mutations that disrupt STAT signalling result in too many or too few migratory cells and poor migration<sup>9–11,21,22</sup>. Thus, precise regulation of STAT activity ensures proper egg chamber development.

One key STAT activity regulator in follicle cells is Apontic (Apt). Apt is widely expressed and serves as a feedback inhibitor of STAT signalling<sup>19,20,23</sup>. In loss-of-function *apt* mutants, anterior follicle cells activate STAT to a greater extent than normal, resulting in additional motile cells. Thus, Apt normally sets a high threshold for STAT-activated motility, and acts to shut off STAT function in cells with intermediate or low levels of

activation. This genetic inhibition limits the number of motile cells specified in the anterior epithelium.

Upd secreted apically by the polar cells diffuses beneath the epithelium<sup>14</sup> into an extracellular domain bounded by the neighbouring nurse cells. Because the nurse cells are very large, their membranes create an irregular region adjacent and subapical to the follicle cells (Fig. 1a,b). To investigate whether this landscape of neighbouring tissue influences morphogen-mediated cell fate decisions in the follicular epithelium, we developed a new strategy to view egg chambers<sup>24</sup>. This protocol positions the polar cells above the nurse cells, providing a unique perspective. If the contour of the adjacent germline cells did not alter morphogen signalling, we would anticipate uniform STAT activation around the polar cells when viewed upright; in contrast, asymmetry in cell fate patterning could suggest influence by the nurse cells or the irregular extracellular domain they create.

We found significant variation among the patterns of Slbo and STAT expressing cells in the anterior epithelium, creating striking asymmetry in specification of motile cells. Genetic analysis shows that this variation is affected by the levels of STAT activity. Because Upd is released into an often-irregular domain bounded by nurse cells, we postulate that the landscape of adjacent tissue influences local morphogen concentrations and thereby cell fates. Simulations from our three-dimensional (3D) mathematical model of Upd dynamics and STAT activation in this cellular context support our hypothesis. Examination of mutant egg chambers with altered nurse cell arrangements and subapical architecture further indicates that cellular landscape influences morphogen distribution and adjacent cell fates. While the egg chamber provides a simple case, this work has broad implications in understanding the effects of diffusible signalling molecules more generally.

## Results

### Upright imaging reveals multiple patterns of cell activation.

Developing egg chambers are connected in ovarioles and are oblong, so they are generally viewed lying on their lateral side, obscuring cell fate patterning at the poles. Thus, the early organization of the border cells around the polar cells has not been clearly shown. During stage 8 of oogenesis, presumptive border cells arise near the polar cells in response to secreted Upd. Lateral views of egg chambers indicated that cells in contact with polar cells are fated to become migratory border cells, whereas those further away are fated as non-motile anterior follicle cells. This led to the conventional wisdom that the activated cells are arranged radially around the polar cells, and that all cells in contact with polar cells should be activated.

To observe the pattern of border cell specification at the anterior, we developed a method to observe egg chambers end-on<sup>24</sup>. We first used the genotype *slbo-Gal4, UAS-mCD8-GFP* (referred to here as the *slbo* reporter; refs 25,26 and Fig. 1a) to mark the border cells, which reveals the Slbo expression gradient across the anterior epithelium. We manually sorted and mounted individual egg chambers in glycerin jelly standing with the anterior end facing up (refs 24,27 and Fig. 1b). We visualized horizontal cross-sections of vertical, late stage 8 egg chambers across multiple focal planes, revealing each cell of the anterior epithelium. When viewed upright, we expected every cell in contact with the polar cells to have activated STAT and also to express its target *slbo*.

Interestingly, we found several different arrangements of presumptive border cells around the polar cells, assayed using the *slbo*-reporter line. In 25% of stage 8 egg chambers, *slbo*-positive cells formed a ring surrounding the polar cells in

the expected radial pattern, and all cells contacting the polar cells were positive (Fig. 1c and Supplementary Fig. 1). This configuration is consistent with the prediction that arises from postulating that Upd diffuses isotropically from a local source to activate JAK/STAT, and thus Slbo. Surprisingly, we found that a larger percentage of egg chambers (29%) revealed presumptive border cells all organized to one side of the polar cells (Fig. 1d and

Supplementary Fig. 1). In this case, only a few *slbo*-positive cells directly contacted the polar cells (Fig. 1d). This asymmetric pattern is contrary to what is expected if the polar cells release Upd and it diffuses evenly away, since follicle cells neighbouring the polar cells remained negative for *slbo* expression.

We found a diversity of *slbo*-positive cell arrangements in the anterior epithelium. We grouped stage 8 egg chambers into four

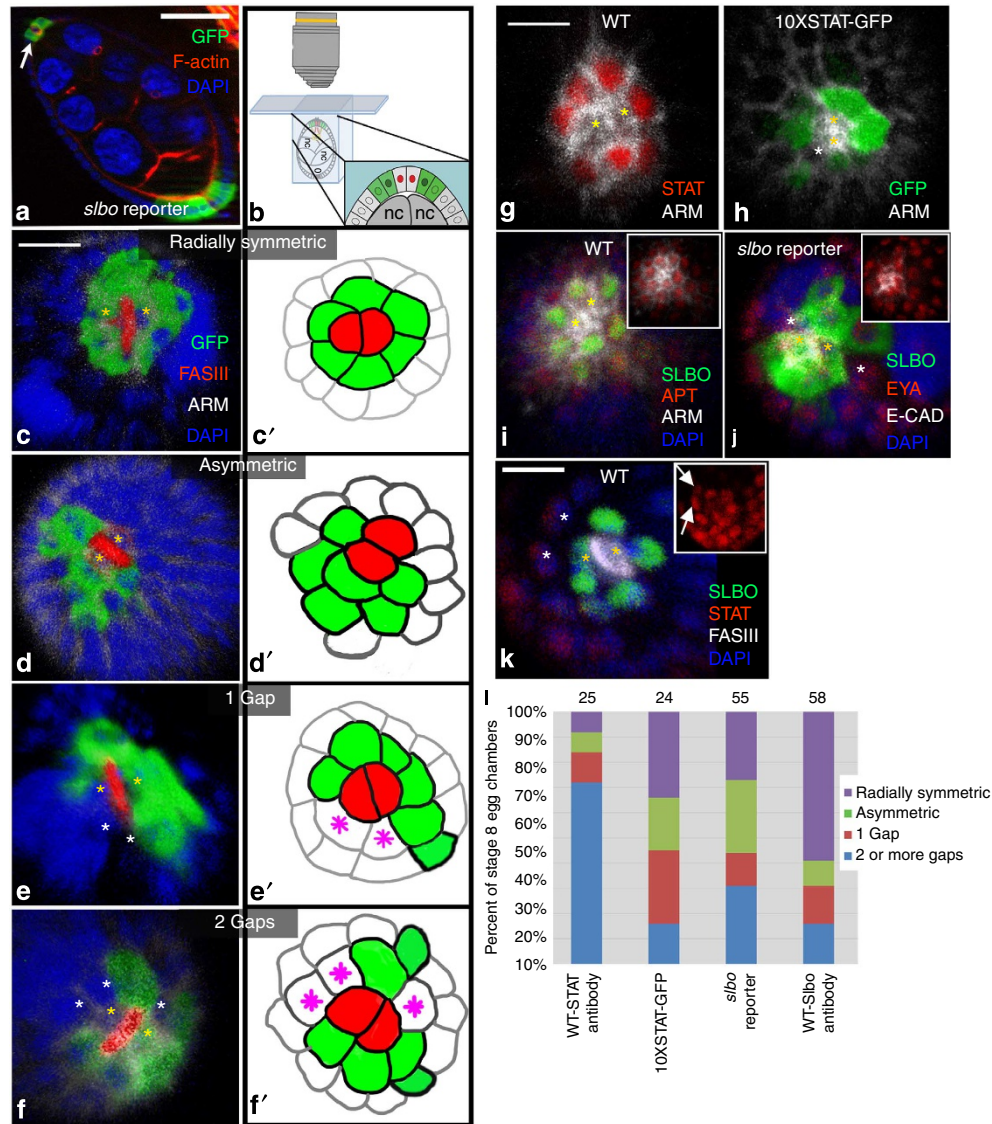


**Figure 1 | Upright imaging reveals multiple patterns of STAT activation in follicular epithelia.** (a) Lateral view of a stage 8 *slbo*-reporter egg chamber; presumptive border cells are GFP positive (green, arrow), F-actin (phalloidin) is shown in red and nuclei (4,6-diamidino-2-phenylindole (DAPI)) are blue. Scale bar, 50  $\mu$ m. (b) Schematic of upright egg chamber imaging technique. Inset shows presumptive border cells (green), polar cells (red nuclei), nurse cells (nc), and the extracellular subapical space between the epithelium and nurse cells (white). (c–k) Three-dimensional reconstructions of optical sections, projected into one plane, from the anterior epithelia of stage 8 egg chambers. Yellow asterisks mark polar cells. Scale bar, 10  $\mu$ m. (c–f) Egg chambers from *slbo*-reporter (GFP, green) flies. White asterisks mark ‘gap cells’: GFP-negative cells contacting the polar cells. Fasciclin III (Fas III) is red; Armadillo (Arm), white; DAPI, blue. See also Supplementary Fig. 1. (c’, f’) Schematics of cell organizations. Polar cells, red; presumptive border cells, green; gap cells, magenta asterisks. (c’, e’) Radially symmetric organization of *slbo*-positive cells. (d’, f’) Asymmetric organization of *slbo*-positive cells. (e, e’) One gap in *slbo*-positive cells around the polar cells. (f, f’) Two gaps in organization of *slbo*-positive cells. (g) STAT expression (red) is radially symmetric around the polar cells in seven neighbouring cells in wild type (WT; Canton S). (Arm, white.) (h) STAT activity (green) shows one gap around the polar cells, indicated by lack of 10XSTAT-GFP expression (white asterisk). (Arm, white.) (i) Seven Slbo-expressing cells (green) radially symmetric around the polar cells (yellow asterisks) in wild type. Apt, red, inset; Arm, white; DAPI, blue. (j) Two gaps (white asterisks) in *slbo*-reporter activation (green) next to the polar cells (yellow asterisks). Eyes absent (Eya), red, inset; E-cadherin (E-CAD), white; DAPI, blue. (k) Slbo protein (green) present in cells to one side of polar cells (yellow asterisks) (Fas III, white) and absent from two cells (white asterisks), although STAT (red, inset, arrows) is detected. (l) Proportions of four classes of organization patterns in the first tier of cells contacting the polar cells using four different markers/genotypes (bottom). For *slbo* reporter and 10XSTAT-GFP, positive cells were scored by GFP antibody staining. Numbers of egg chambers scored (n) shown at the top.

categories according to the activation pattern of the first tier of cells surrounding the polar cells: radially symmetric, asymmetric (activated to one side, both described above), one gap and two gaps or more (Fig. 1c'–f,l). The one gap class displayed one or two follicle cells in direct contact with the polar cells but not expressing *slbo* (Fig. 1e). The two or more gap arrangement was classified by appearance of two or more cells in contact with polar cells that did not express *slbo*, and did not contact each other (Fig. 1f). We only scored egg chambers with at least five positive cells to avoid younger stages, and because that was the smallest number of cells that could completely surround the polar cells. We observed similar total numbers of STAT-activated, *slbo*-positive cells in all arrangements, on average  $6.5 \pm 0.6$  s.e.m. (Table 1). Notably, this is similar to the total number of follicle cells in direct contact with polar cells, which for this genotype was  $6.5 \pm 0.2$  s.e.m., and was consistent over different activation patterns (Table 1). Thus, most arrangements of border cell precursors are not radially symmetric with respect to the polar cells.

We used different markers to observe the specification patterns of border cells in detail. Examining STAT expression in wild-type (Canton S) egg chambers, or green fluorescent protein (GFP) expression in the STAT activity reporter line, 10XSTAT-GFP<sup>28</sup>, we found the same diversity in presumptive border cell arrangements as seen in the *slbo*-reporter line (Fig. 1g,h,k,l), and similar total numbers of positive cells (Table 1). We also assayed egg chambers from a wild-type strain labelled with an antibody that detects Slbo protein. Again, we observed the same patterns of arrangements (Fig. 1i–l) and similar numbers of activated cells at stage 8 (Table 1). We noticed some differences between the genotypes and markers, probably owing to slight differences in the timing of expression; from prior work<sup>5</sup>, we expect that STAT and its activity reporter would be activated first, followed by *slbo* reporter and then Slbo protein, which requires a high level of STAT activity (and therefore Upd) to be activated. It is also possible that the markers are differentially sensitive to detection, but we do not think this explains the different patterns observed because similar numbers of total presumptive border cells were detected in each case (Table 1), and asymmetric patterns persisted into later stages (Supplementary Fig. 2). Upon

additional quantification, we found no significant difference between genotypes in the proportion of egg chambers exhibiting radial symmetry of Slbo-positive cells about the polar cells (using a  $\chi^2$ -contingency test,  $P$  value  $> 0.05$ ; Fig. 1l).

Using several markers, many egg chambers exhibited asymmetry of motile cell fate acquisition. In contrast, all anterior cells displayed expression of the STAT-negative regulator Apt (Fig. 1i, inset), demonstrating that all cells are viable and equally visible by this imaging method. Follicle cell marker Eyes Absent (*Eya*) was also evenly expressed across the epithelium (Fig. 1j, inset), further indicating that these anterior cells are all normal. Thus, surprisingly, some cells in contact with the polar cells fall below the STAT activity threshold necessary for border cell specification, demonstrated by the lack of nuclear STAT, STAT reporter expression or expression of the STAT target, Slbo.

**Raising STAT activity increases radial symmetry.** We considered several possibilities for how the asymmetry in presumptive border cell specification might occur. If too few cells became activated, this would generate asymmetry around the polar cells; however, contrary to this idea, we found in most genotypes 6–7 follicle cells contacted the polar cells, and in the majority of egg chambers at least this many presumptive border cells were activated (Table 1). It was possible that one polar cell secreted much higher levels of Upd, however, this would result in the negative cells to be always oriented to one side of the polar cell pair, which was not the case (for example, Fig. 1d–f,j,k). Another explanation for asymmetric activation of STAT around the polar cells could be intrinsic differences between cells of the epithelium, such as lack of Dome expression in some, or localized expression of an inhibitor. We did not observe obvious differences in *dome-lacZ* reporter expression across the anterior epithelium (refs 7,9,29 and Supplementary Fig. 3).

To determine whether some follicle cells were refractory to STAT activation, we altered signalling levels. Genetic disruption of the negative regulator *apt* increases STAT activity in the anterior epithelium<sup>19</sup>. In upright egg chambers from flies homozygous for a loss-of-function mutation in *apt* (*apt*<sup>KG05830</sup>), we saw significantly more Slbo-expressing cells at stage 8 than in controls ( $11.6 \pm 0.5$  versus  $6.1 \pm 0.7$  s.e.m.;  $P < 0.0001$  by ANOVA; Fig. 2a compare with Fig. 1f), which is consistent with prior results. Most *apt* mutant egg chambers exhibited a radial organization of Slbo-expressing cells around the polar cells, a significant increase in this arrangement compared with controls (Fig. 2a,f;  $P < 0.0001$  in a  $\chi^2$ -contingency test). Almost all cells in contact with the polar cells were positive for Slbo and STAT in this genotype (Fig. 2a,f and Supplementary Fig. 4). This demonstrates that all cells in this region are capable of STAT activation.

Next, we raised STAT activity in follicle cells by increasing Upd expression<sup>9–12,21</sup>. In the anterior epithelium, *upd* transcripts localize to the apical side of the polar cells<sup>14</sup>, but there is no report of asymmetry of Upd in other axes. We overexpressed Upd in the polar cells using the *upd-Gal4* driver and two different overexpression transgenes (UAS-*Upd21.6* and UAS-*Upd26.2*; ref. 21). With higher extracellular Upd, egg chambers exhibited radial symmetry of STAT activation about the polar cells much more often than controls (Fig. 2b,c,f and Supplementary Fig. 4). In this case, cells that normally display low levels of STAT activation showed higher activity, indicated by high expression of Slbo protein, and significantly more cells had Slbo expression than in controls ( $8.6 \pm 0.3$  versus  $6.1 \pm 0.7$  s.e.m.,  $P < 0.001$ ). These results imply that few, if any, of the anterior follicle cells are intrinsically refractory to STAT activation, and suggest that a different mechanism must explain the asymmetric specification of border cells.

**Table 1 | Presumptive border cell number across organization.**

Genotype	Positive cells contacting PC	Total FC contacting PC	Total positive cells	Organization
10XSTAT reporter ( <i>n</i> = 24)	$5.8 \pm 0.2$	$6.8 \pm 0.2$	$8.6 \pm 0.7$	1 Gap
	$4.1 \pm 0.3$	$7.1 \pm 0.2$	$7.9 \pm 0.7$	2 Gaps
	$5.0 \pm 1$	$8.5 \pm 0.5$	$6.0 \pm 2.0$	Asymmetric
<i>slbo</i> reporter ( <i>n</i> = 55)	$6.8 \pm 0.5$	$6.8 \pm 0.5$	$8.0 \pm 1.7$	Radial
	$4.9 \pm 0.3$	$6.1 \pm 0.3$	$5.8 \pm 0.4$	1 Gap
	$3.9 \pm 0.3$	$6.6 \pm 0.2$	$5.8 \pm 0.4$	2 Gaps
WT-Slbo antibody ( <i>n</i> = 58)	$4.1 \pm 0.3$	$6.0 \pm 0.3$	$6.1 \pm 0.5$	Asymmetric
	$6.8 \pm 0.4$	$6.8 \pm 0.4$	$8.4 \pm 0.7$	Radial
	$5.3 \pm 0.02$	$6.0 \pm 0.5$	$7.0 \pm 0.5$	1 Gap
	$4.0 \pm 1.0$	$6.5 \pm 0.5$	$5.0 \pm 0.0$	2 Gaps
	$4.0 \pm 0.0$	$7.0 \pm 0.4$	$5.0 \pm 0.6$	Asymmetric
	$5.9 \pm 0.1$	$6.0 \pm 0.1$	$7.5 \pm 0.3$	Radial

FC, follicle cell; GFP, green fluorescent protein; PC, polar cell; WT, wild type. Presumptive border cell numbers were scored by upright imaging of egg chambers from the indicated genotypes, with the Canton S strain for WT. Cells positive for GFP or Slbo protein expression by antibody staining were scored as positive. Fasciclin III expression was used as a marker for the PCs and DAPI DNA dye revealed all FCs in the domain. Error is given as s.e.m., and the number of egg chambers assayed is indicated with *n* = for each genotype. Additional statistical analysis is shown in the text and Fig. 1. Organization was determined as described in the text.

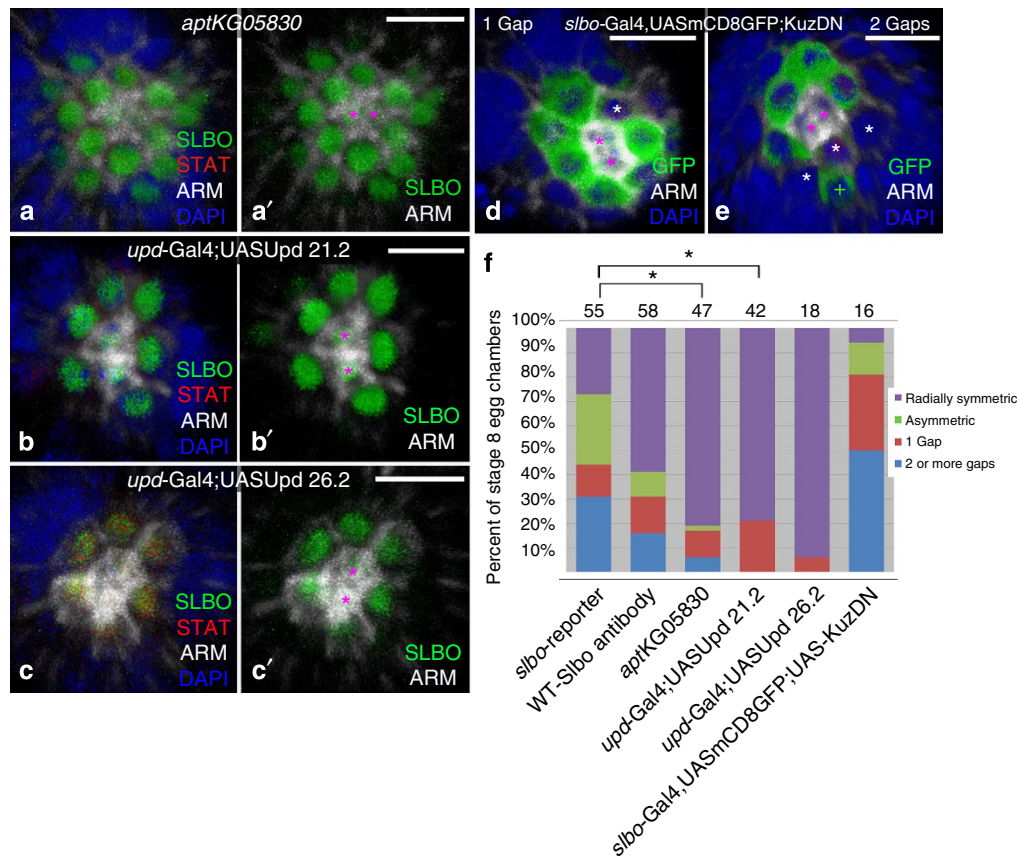


**Figure 2 | Increased STAT activity increases radial symmetry in border cell specification. (a–e)** Three-dimensional reconstructions of optical sections, projected into one plane, of anterior epithelia of mutant stage 8 egg chambers. Magenta asterisks indicate polar cells, whereas white asterisks indicate gap cells. Scale bars, 10  $\mu$ m. **(a–c)** Slbo protein, green; STAT, red; Armadillo (Arm), white; 4,6-diamidino-2-phenylindole (DAPI), blue. See also Supplementary Fig. 4. **(a)** An egg chamber from an *apt<sup>KG05830</sup>* homozygote shows radial symmetry of Slbo-positive cells in the first tier of cells around the polar cells. **(b,c)** Overexpression of Upd in polar cells results in radial symmetry of Slbo-positive cells around the polar cells with either of two transgenes: *upd-Gal4; UAS-Upd 21.2* **(b)** or *upd-Gal4; UAS-Upd 26.2* **(c)**. **(d,e)** *slbo-Gal4, UAS-mCD8-GFP; UAS-Kuz<sup>DN</sup>* egg chambers display one **(d)** and two gaps **(e)** in border cell-specification patterns. GFP, green; Arm, white; DAPI, blue. The case in **e** is classified as two gaps because one gap cell touches the polar cells and a second is between the polar cells and a distant *slbo*-positive cell, indicated with a green +. **(f)** Proportions of four classes of arrangements of presumptive border cells at stage 8 for the following genotypes and markers: *slbo-Gal4* reporter line (using GFP), wild type (Slbo antibody staining), *apt<sup>KG05830</sup>* (Slbo staining), *upd-Gal4; UAS-Upd 21.2* (Slbo staining), *upd-Gal4; UAS-Upd 26.2* (Slbo staining), *slbo-Gal4, UAS-mCD8-GFP; UAS-Kuz<sup>DN</sup>* (GFP antibody staining). Numbers of egg chambers scored are listed at the top of each column. A significant difference is indicated by \* $P < 0.0001$ , in a  $\chi^2$ -contingency test.

**Asymmetry in activation does not require Notch signalling.** Delta-Notch signalling is generally known for creating cellular heterogeneity during development and is necessary for cell specification in *Drosophila*<sup>6,8,30,31</sup>. During early oogenesis, Notch signalling regulates polar and follicle cell differentiation<sup>32–35</sup>. The Kuzbanian (Kuz) metalloproteinase cleaves and activates Notch and is highly expressed in the border cells<sup>36,37</sup>. Kuz, Delta and Notch are all required for normal border cell migration<sup>37,38</sup>. Thus, we considered whether Notch signalling influenced the asymmetry of cell specification. We inhibited Notch in border cells by expressing dominant-negative Kuz (referred to as *Kuz<sup>DN</sup>*)<sup>39</sup> during mid-oogenesis. We observed that all the STAT activation patterns seen in control egg chambers, including asymmetry, exist in *Kuz<sup>DN</sup>* mutants (Fig. 2d–f), and in similar proportions to controls (no significant difference between pattern distributions by  $\chi^2$ -contingency tests). Eighty-one percent of mutant stage 8 egg chambers exhibited at least one gap in activation around the polar cells (Fig. 2f). *Kuz<sup>DN</sup>* egg chambers had the same number of Slbo-positive cells as controls (average of 6.0 versus 5.8, respectively, not significantly different in a two sample *t*-test,  $P > 0.05$ ), illustrating little or no change in the

STAT threshold in the anterior epithelium. Thus, Notch signalling is unlikely to be required for asymmetry, although we cannot rule out that there may be some contributions from this pathway.

**Underlying tissue architecture affects response to Upd.** Our experiments demonstrated that STAT activity levels influence the border cell-specification patterns observed (Fig. 2a–c,f). We hypothesized that the asymmetric STAT activation in the epithelium could be caused by an uneven distribution of the Upd signalling molecule owing to the irregular domain created by the contours of the underlying tissue. The single-layer follicular epithelium lies above a cluster of large nurse cells (Fig. 1a,b, inset). Anterior polar cells secrete Upd extracellularly towards the nurse cells, which do not significantly express the Upd receptor Dome (Supplementary Fig. 3). While the nurse cells are generally space filling, regions where two or more cells meet create small extracellular domains or clefts (Fig. 1b inset). Thus, the edges of the nurse cells could influence how Upd is distributed in the subapical extracellular domain and received by epithelial cells.

We used markers for nurse cell boundaries and anterior imaging to visualize the domain adjacent to the epithelium. We stained egg chambers with fluorescent phalloidin to mark membrane-associated cortical actin, which provided an estimate for the cell edges. Although the clefts created by nurse cells varied in size, they appeared widest close to the epithelium and narrowed quickly towards the interior of the egg chamber (Fig. 3a,b), and tended to be smaller than a follicle cell. These subapical regions were roughly triangular in cross-section, and measured  $10.7\mu\text{m}^2$  on average in the focal plane of polar cells when analysed in laterally imaged egg chambers ( $n=14$ ; Fig. 3a–b' and Supplementary Table 1, and see Methods section). We observed similar size clefts in upright 3D reconstructions (Supplementary Movie 1). Although we observed several different arrangements, in 11% of wild-type egg chambers, one nurse cell juxtaposed the epithelium near the polar cells. More commonly (38% of cases), three nurse cells were positioned adjacent to the anterior-most follicular epithelium (assayed by nurse cell nuclei

in the *slbo*-reporter genotype,  $n=38$ ). We analysed in more detail the simple situation when the polar cells sat directly over a single nurse cell. In 4/7 of these cases, the STAT activation pattern was radially symmetric (for example, Fig. 3c–c''', Supplementary Fig. 5, Supplementary Movie 1 and Supplementary Table 2), consistent with Upd being relatively evenly distributed. However, in 3/7 of these egg chambers, some presumptive border cells sat over or near a cleft, and a gap in STAT activity was observed (Supplementary Table 2). More complexity in patterns arose when more than 1 nurse cell lay in the anterior-most region of the egg chamber. When polar cell position aligned near a cleft created by two nurse cells, the STAT activation pattern had gaps and asymmetries (Fig. 3d–e''', and Supplementary Movies 2 and 3). In multiple cases, follicle cells over prominent clefts showed no activation (Fig. 3e'''), which might be expected if the extracellular domain acted as a sink for Upd. However, in some cases, follicle cells over clefts created by nurse cells did show activation, even if they were several cell diameters from the polar cells (Fig. 3d''' and

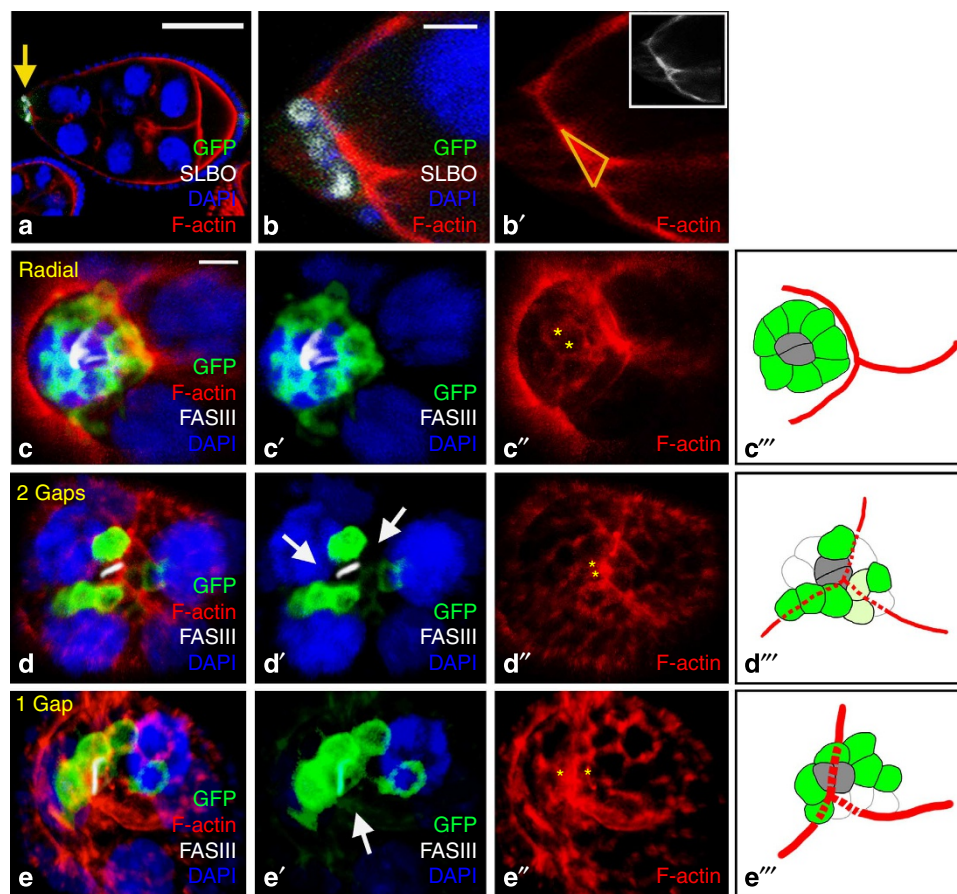


**Figure 3 | Cell-specification patterns relative to adjacent nurse cell positions.** (a–e) Staining for F-actin (with phalloidin, red) shows cell contours in stage 8 *slbo* reporter line egg chambers. (a) Wild-type egg chamber viewed laterally shows presumptive border cells at the anterior marked by *Slbo* expression (white, yellow arrow) and GFP (green). Scale bar, 50  $\mu\text{m}$ . (b,b') Magnified view of the anterior of the egg chamber shown in a; a subapical cleft created by the nurse cells can be seen adjacent to the activated cells. Scale bar, 10  $\mu\text{m}$ . Yellow triangle in b' shows the region measured to approximate the cleft dimensions (width along the apical side of the epithelium, depth from epithelium to where nurse cells meet). Inset shows F-actin staining alone. (c–c'',d–d'',e–e'') Projections of optical sections from the anterior of egg chambers, including epithelium and top of underlying nurse cells. White arrows indicate gap cells. Yellow asterisks indicate polar cells. *slbo* reporter, GFP, green; F-actin, red; Fasciclin III (Fas III), white; 4,6-diamidino-2-phenylindole (DAPI), blue. Scale bar is 7  $\mu\text{m}$ . (c''', d''', e''') Schematics of presumptive border cell organization in the anterior epithelium. Polar cells are grey, presumptive border cells are green, presumptive border cells with low GFP expression are light green, gap cells are outlined in light grey, and the nurse cell cleft is red. Dotted portion of the cleft indicates the portion underlying anterior follicle cells. (c–c''') Radially symmetric organization of *slbo*-positive cells. Polar cells and presumptive border cells positioned above nurse cell nuclei, with Y-shaped cleft to the right (see also Supplementary Fig. 5). (d–d''') Two gaps in organization of *slbo*-positive cells around the polar cells. Polar cells positioned above the nurse cell cleft; arrows indicate gap cells touching polar cells. (e–e''') One gap organization of *slbo*-positive cells around the polar cells. Polar cells positioned near the nurse cell cleft; arrow indicates gap cell region. See also Supplementary Movies 1–3.

Supplementary Movie 2). How Upd might create this pattern was less clear. We were unable to examine Upd protein directly, as a fluorescently tagged reporter was not bright enough *in vivo*, and examination of extracellular protein in fixed tissue would not reveal signals where there are gaps between cells. Thus, to address our hypothesis, we developed a mathematical model.

### A computational model explains asymmetric Upd distribution.

To model Upd distribution in the 3D extracellular space, we used a partial differential equation that accounts for the change in Upd concentration over time due to the secretion, diffusion and uptake rates of this activator:

$$\frac{\partial u}{\partial t} = \nabla \cdot (D \nabla u) = D \left( \frac{\partial^2 u}{\partial x^2} + \frac{\partial^2 u}{\partial y^2} + \frac{\partial^2 u}{\partial z^2} \right), (x, y, z) \in \Omega \quad (1)$$

$$-D \frac{\partial u}{\partial z} \Big|_{\text{apical side of polar cells}} = \sigma \quad (2)$$

$$-D \frac{\partial u}{\partial z} \Big|_{\text{apical side of follicle cells}} = -ku \quad (3)$$

$$-D \nabla u \cdot \mathbf{n} \Big|_{\text{all other boundaries}} = 0 \quad (4)$$

for outward normal vector,  $\mathbf{n}$ , where  $D$  represents the diffusion coefficient ( $D = 1 \mu\text{m}^2 \text{s}^{-1}$ ; which is within the range of diffusion coefficients determined for similar-sized molecules in *Drosophila*, as in refs 40,41). We estimated that Upd is released from the apical side of both polar cells at a rate of  $\sigma$  ( $\sigma = 45 \text{pM} \mu\text{m} \text{s}^{-1}$ , see Methods section), diffuses and is taken up by all follicle cells at the rate  $-ku$  with uptake proportionality constant  $k$  ( $k = 1 \times 10^{-4} \text{s}^{-1}$ ). (Since nurse cells had undetectable expression of the Upd receptor, we did not include uptake along this surface.) The source term was determined as the value necessary to achieve a threshold concentration of 3,900 pM, based on cell culture experiments<sup>42</sup>, and the uptake proportionality constant was converted to units of surface flux. We defined the domain of subapical extracellular space,  $\Omega$ ,  $((-50 \mu\text{m}, 50 \mu\text{m}) \times (-50 \mu\text{m}, 50 \mu\text{m}) \times (0 \mu\text{m}, -0.2 \mu\text{m}))$ , that is bounded at the top by the apical surface of the epithelium, and at a distance,  $d$ , below by nurse cells (Fig. 4a,b, see Methods section), using no-flux boundary conditions outside of the polar and follicle cells. In the base case,  $d = 0.2 \mu\text{m}$ . We estimate a follicle cell surface size to be  $5 \mu\text{m} \times 5 \mu\text{m}$ . We refer to the space created by two juxtaposed nurse cells as the ‘cleft’ (length  $\times$  width  $\times$  depth). We considered cases in which one, two or three nurse cells were adjacent to the epithelium, and varied cleft dimensions accordingly. A 3D spatio-temporal simulation was then performed to estimate the concentration of Upd at all points in the domain.

The computational model was run for different lengths of time and a range of hypothetical source terms to see the effects on morphogen distribution over time. We set Upd concentration to 0 pM at time zero, and set a threshold level of 3,900 pM for the concentration sufficient to activate and maintain STAT signalling, as this is consistent with physiological levels in cell culture<sup>42</sup>. We generated contour plots to determine the morphogen concentration at the apical epithelial boundary (where  $z = 0 \mu\text{m}$  in the domain; Fig. 4a). As expected, when modelled with an even underlying domain (no cleft; Fig. 4b), Upd signal at a concentration higher than 3,900 pM arose in a radially uniform ring around the polar cells (Fig. 4c), which would activate STAT in surrounding cells. Since the model is linear up to the source term, increasing  $\sigma$  increases the concentration at the epithelial surface (and increases the likelihood of activating more cells, as in Upd overexpression; Fig. 2, and see below). Increasing  $D$  would increase the spread of Upd in the same amount of time, and

increasing  $k$  would decrease the spread of Upd by increasing the uptake. As a first test, we also explored the outcome when only one polar cell secreted Upd (Supplementary Fig. 6). As we expected, follicle cells nearest to the secretory polar cell became activated, whereas those to the other side were not (Supplementary Fig. 6c). However, there is no evidence one polar cell is inactive, and since our asymmetric patterns of activation *in vivo* did not consistently align to one side of the polar cell pair, this idea did not explain the majority of the asymmetries we observed.

Next, we introduced different underlying cleft geometries into the computational model to see how this affected Upd distribution and cell activation. We began with a simple case: two nurse cells and one cleft under the polar cells (Fig. 4d). In this case, a  $7 \mu\text{m}$ -wide cleft acted as a sink in short time frames (2.5 h), shifting high STAT activation to the other side of the polar cells only (indicated by the heat maps in Fig. 4e), even though both cells secreted Upd. At longer times (6 h), a different asymmetry was observed: higher levels of Upd expanded along the cleft, potentially at high enough levels for border cell specification along that domain (Fig. 4e'). This suggests that once Upd is released into the cleft, it fills up the ‘sink’ and then disperses into the surrounding area. At late times, this crevice behaves as a source of Upd, although at a lower level than the polar cells.

We next replicated the common three nurse cell arrangement in the computational model to determine how this impacted Upd distribution. This organization of nurse cells leads to a Y-shaped crevice (Fig. 4f,g). In this case, we performed a parametric sweep by altering the dimensions of a single branch of the cleft to range between 0.5 and  $5 \mu\text{m}$  in depth and width, respectively. This size range, because it is modelled as a rectangular prism domain, roughly maps to the volume of the concave triangular prism domains observed in egg chambers. Over this range, the computational model unexpectedly yielded all four cell-specification patterns observed *in vivo* (Fig. 4h,i). If we significantly increased the source term ( $\sigma = 75 \text{pM} \mu\text{m} \text{s}^{-1}$ ) to represent overexpression of Upd (as in Fig. 2), radial symmetry was restored even when including a Y-shaped cleft (Supplementary Fig. 7). Thus, our model implies that underlying tissue contour alters how morphogens signal to adjacent tissue, and thereby modulates cell-specification patterns.

### Enlarged subapical domain results in symmetrical activation.

To test further the hypothesis that underlying tissue geometry influences morphogen distribution, we examined mutant egg chambers that had fewer nurse cells. Specifically, we used mutant alleles of the gene *half pint* (*hfp*; which encodes Poly U binding factor 68kD), in which nurse cells often fail to complete the correct number of cell divisions<sup>43,44</sup>. We confirmed that females bearing viable combinations of two different mutant alleles (*hfp*<sup>38</sup>/*hfp*<sup>13</sup>), or heterozygous mutant females for a strong allele (*hfp*<sup>13</sup>/+), developed stage 8 egg chambers that had fewer than the normal 15 nurse cells, averaging 10.8 or 12.0, respectively (Fig. 5a;  $n = 16$ ). We did not detect any abnormalities in gross follicle cell development using these alleles (Fig. 5b and Supplementary Fig. 8), which is consistent with prior reports that primarily germline cells are disrupted<sup>43</sup>.

Presumptive border cell activation patterns in *hfp* mutant egg chambers differed significantly from controls, with 100% of stage 8 egg chambers exhibiting radial organization of Slbo-expressing cells (compare Fig. 5c with Fig. 1c–f). In 41% of egg chambers examined (7/16), only one nurse cell juxtaposed the anterior epithelium, and, as in the ‘no cleft’ case, all of the follicle cells contacting the polar cells were positive for markers of STAT activity, including Slbo and STAT proteins (Fig. 5c). Remaining

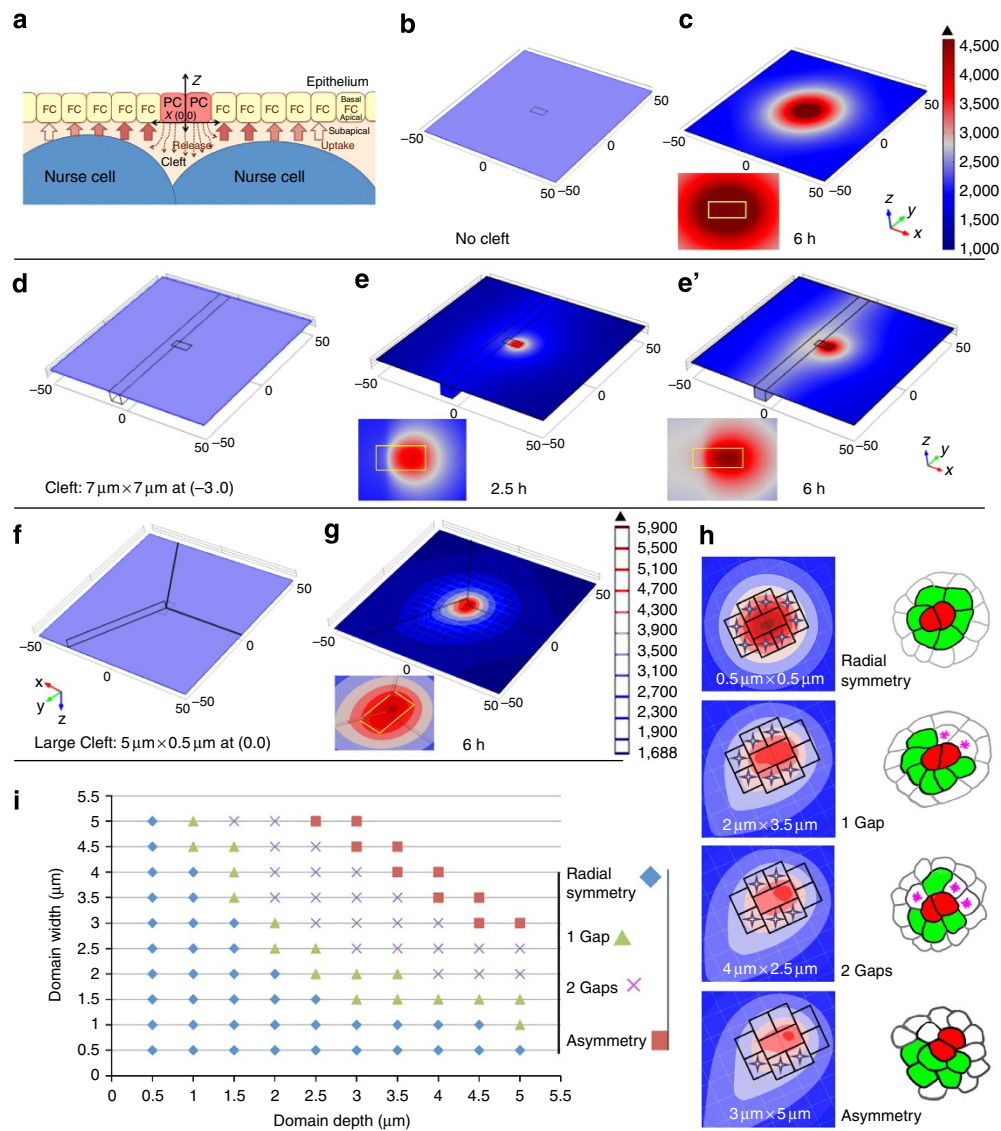


**Figure 4 | Nurse cell landscape alters STAT signalling levels and cell-specification patterns.** **(a)** Diagram shows follicle cells (FCs, yellow), polar cells (PCs, red), and adjacent nurse cells (blue), which create a cleft in the extracellular space (exaggerated for clarity). Domain coordinates are set to (0,0,0) at the apical point between PCs. PCs secrete Upd (dashed arrows). Upd uptake depends on its local concentration; darker red arrows indicate more uptake, whereas lighter arrows indicate less uptake. **(b,d,f)** Representations of the domain at the apical surface of the epithelium spanning 50  $\mu\text{m}$  from the centre (PCs, rectangle). **(b)** A flat domain with no cleft. **(c,e,e')** Heat maps show resultant Upd concentrations at the cell apical surface after simulations. Colour scale bar (to the right of **c**) shows highest [Upd] in dark red; lowest in blue; insets magnify the flattened region around the PCs (yellow rectangle). **(c)** After a 6 h simulation, [Upd] is highest radially around the PCs and decreases with increasing distance. **(d)** A domain used for **e** has a rectangular region below one PC to approximate the cleft between two, subepithelial nurse cells, as in **a**. **(e)** Early, [Upd] is high to one side of the PCs and low above the cleft. **(e')** Later, near-threshold levels of [Upd] (grey/pink) appear above the cleft. **(f)** A Y-shaped region centred at (0,0,0) approximates the cleft formed between three nurse cells, shown from the apical side for clarity (axes indicated). The variable-branch domain (left) of the cleft is sized at 5  $\mu\text{m}$  deep  $\times$  0.5  $\mu\text{m}$  wide, and the two constant branches at 0.5  $\mu\text{m}$   $\times$  0.5  $\mu\text{m}$ . **(g)** Simulation using the domain from **f** depicts high [Upd] along the deepest cleft branch (colour scale to the right). **(h)** Simulations using domains with Y-shaped clefts yield the patterns of border cell specification observed *in vivo* (variable-branch size indicated). Cells approximated as 5  $\mu\text{m}$  by 5  $\mu\text{m}$ ; diamonds indicate above-threshold [Upd] (presumptive border cells); scale as in **g**. Schematics as in Fig. 1. **(i)** Different dimensions of the variable branch of a Y-shaped cleft determine different cell-specification patterns via simulations. Regions of the graph lacking points represent sizes for which no activation occurs.

egg chambers predominantly had 2–3 nurse cells at the anterior, but in these cases the nurse cells did not fill the space as completely as in wild type. As a result, a gap was created between the epithelium and the nurse cells (Fig. 5b,d'), generating abnormally large subapical extracellular areas. We estimated this cross-sectional area by measuring a straight-edged crescent shape, excluding the relatively small region of the divot for simplicity (see Fig. 5b, in which the measured domain is outlined). Although this underestimates the total area, we still found the subapical

domain in *hfp* mutants to be significantly larger than in controls, ranging 18–48  $\mu\text{m}^2$  in cross-section (Fig. 5b and Supplementary Table 1). Interestingly, these cases showed normal numbers of presumptive border cells contacting the polar cells, and radially symmetric activation over a larger region, in spite of the large cleft(s) (Table 2).

We next used these data to validate the computational model further. First, we tested the case for one nurse cell near the epithelium and a uniform subapical extracellular domain. As



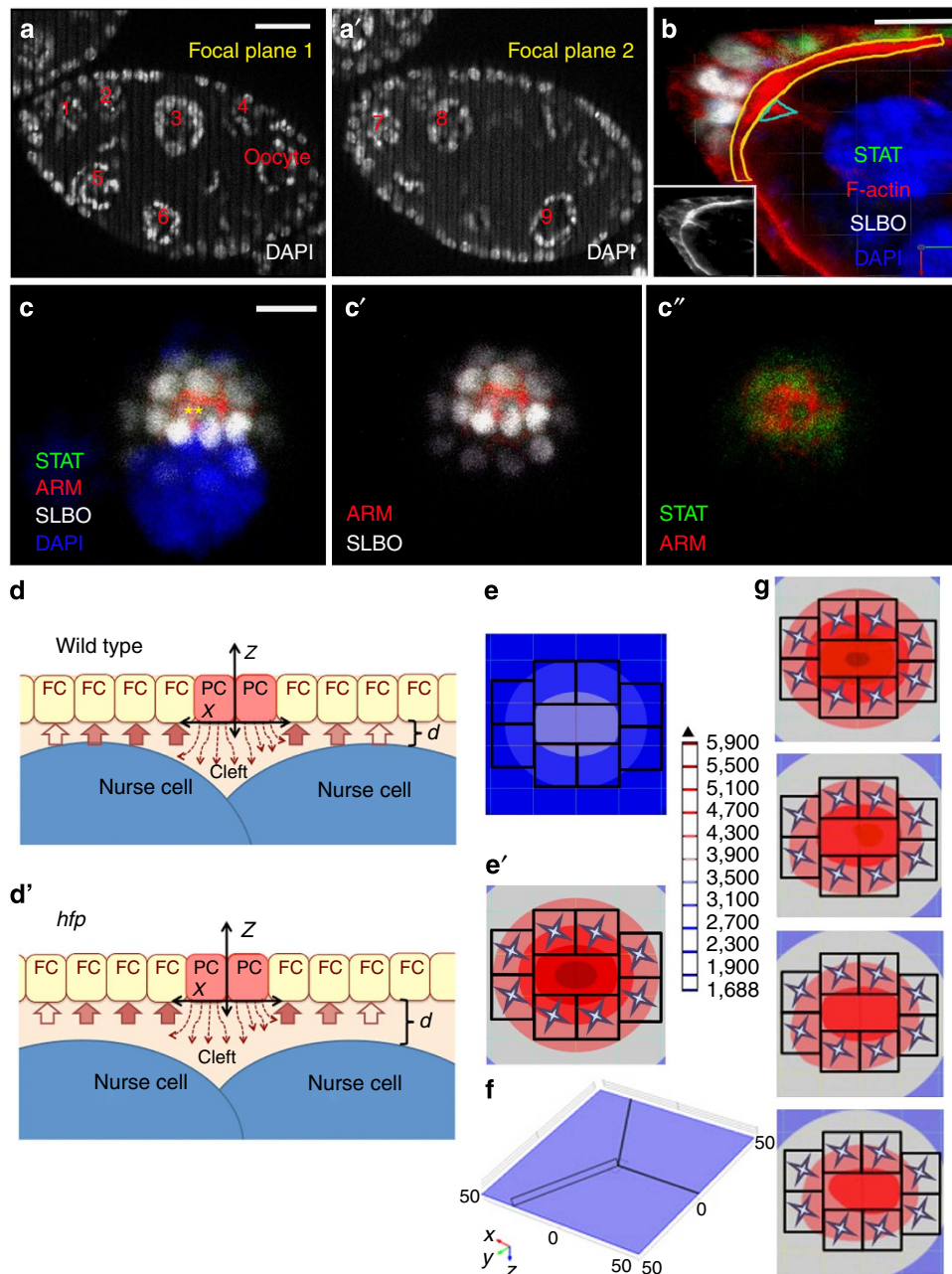


**Figure 5 | Larger extracellular spaces and radially symmetric STAT activation in *hfp* mutants.** (a, a') *hfp*<sup>13</sup>/*TM2* mutant egg chambers contain fewer nurse cells. Nurse cell nuclei, DNA stained with 4,6-diamidino-2-phenylindole (DAPI), are numbered in two focal planes of one egg chamber. Scale bar, 20 μm. (b) A lateral view of the anterior epithelium and nurse cells in an egg chamber from a *hfp*<sup>38</sup>/*hfp*<sup>13</sup> female; phalloidin marks cortical actin (red); DAPI marks DNA (blue); STAT (green) and Slbo (white) expression is detected by antibodies. Nurse cells are not tightly packed against the epithelium, leaving an abnormally large extracellular space (domain outlined in yellow). The cleft domain between two nurse cells is relatively small (cyan outline). Inset shows F-actin staining alone. Scale bar, 10 μm. (c–c'') Anterior of an *hfp*<sup>38</sup>/*hfp*<sup>13</sup> mutant egg chamber. All cells surrounding the polar cells (PCs; yellow asterisks, outlined by Armadillo (Arm) expression, red) have high STAT activation levels, reflected by Slbo (white, c') and STAT (green, c'') expression. In this egg chamber, only one nurse cell lies below the anterior epithelium, seen by DAPI staining. Scale bar, 10 μm. (d, d') Schematics depict the wild-type subapical extracellular domain (d) and that in *hfp* mutants (d'), which is deeper (marked with *d*). (e, e') Simulations to model *hfp* mutants with deeper subapical domains (*d* = 0.5 μm) and no cleft shows no activation when  $\sigma = 45 \text{ pM } \mu\text{s}^{-1}$  (e), but a modest increase in source levels to  $\sigma = 65 \text{ pM } \mu\text{s}^{-1}$  results in radial activation of follicle cells (FCs) (e'), scale to right. (f) A Y-shaped domain with one variable cleft at the left. (g) Simulations to model *hfp* mutants with deeper subapical domains (*d*) and Y-shaped clefts show radially symmetric activation about the PCs for all size variants (scale as in e). Variable-branch sizes: top panel: 0.5 μm wide × 0.5 μm deep, second panel: 2 × 3.5 μm, third panel: 4 × 2.5 μm and bottom panel: 3 × 5 μm.

would be expected, with an increase in subapical space by 2.5 times (or 150%), we saw a decrease in signal strength resulting in no above-threshold cells in the model output (Fig. 5d,e). However, a modest (44%) boost in release strength from 45 to 65 pM μs<sup>-1</sup> results in radially symmetric activation, which is

similar to the case for one nurse cell adjacent to the anterior follicle cells (Fig. 5e'). Moreover, when we modelled this situation with irregular underlying domains, mimicking three nurse cells at the anterior, a similar number of cells were activated but in a radially symmetric pattern for all cleft cases, where one branch of

**Table 2 | Presumptive border cell numbers and arrangements in half pint (*hfp*) loss-of-function mutant egg chambers.**

Genotype	Positive cells contacting PC	Total FC contacting PC	Total positive cells	Organization
<i>hfp</i> <sup>13</sup> , <i>st</i> , <i>cu</i> , <i>e</i> , <i>ca</i> /TM2 ( <i>n</i> = 9)	6.1 ± 0.3	6.1 ± 0.3	12.5 ± 1.1	Radial
<i>hfp</i> <sup>38</sup> , <i>st</i> , <i>cu</i> , <i>e</i> , <i>rec2/hfp</i> <sup>13</sup> , <i>st</i> , <i>cu</i> , <i>e</i> , <i>ca</i> ( <i>n</i> = 7)	6.7 ± 0.3	6.7 ± 0.3	10.7 ± 1.4	Radial

FC, follicle cell; PC, polar cell.  
Presumptive border cell numbers were scored by upright imaging of egg chambers. Cells positive for Slbo protein expression by antibody staining were scored as positive. Fasciclin III expression was used as a marker for the PCs and DAPI DNA dye revealed all FCs in the domain. Error is given as s.e.m., and the number of egg chambers assayed is indicated with *n* = for each genotype. Organization was determined as described in the text.

the Y-shaped cleft is varied (Fig. 5f,g). This modelling result is consistent with the subapical spacing measured in the 2D view, and the increased symmetry in the activation pattern found experimentally in the *hfp* mutants with a smaller numbers of nurse cells. These results validate the computational model and further support the importance of the proximity of the nurse cells in guiding extracellular signalling.

## Discussion

Previous studies suggested that the follicle cells closest to the polar cells receive the highest levels of Upd, maintain above-threshold STAT activity and therefore become fated as migratory<sup>9–12,19</sup>. This implies that proximity to the polar cells is critical to border cell specification. We find that contact with the polar cells is not sufficient to lead to border cell fate. Some follicle cells touching the polar cells do not achieve above-threshold levels of STAT activation. These ‘gap’ cells are of normal follicle cell lineage, indicated by the presence of Apt and Eya proteins, and are capable of receiving signal, as shown when we increased STAT signalling levels. We found no evidence of cell death assayed by activated caspase 3 (ref. 45) staining (Supplementary Fig. 9), and the position of the unactivated cells varied in their alignment with the two polar cells. Differences in the patterns of GFP-marked cells and endogenous proteins in some cases (for example, Fig. 1k), and discontinuities between GFP-positive cells (as in Figs 1h,j and 2e) suggest that movement between follicle cell ring canals<sup>46</sup> is not sufficient to explain asymmetries either. Moreover, asymmetric border cell patterns persist into stage 9, which suggest that cell rearrangement is unlikely to cause the asymmetries (Supplementary Fig. 2). We propose that the cells negative for Slbo expression at stage 9, but in contact with polar cells, dissociate from the border cell cluster and are fated to become stretch cells.

We favour the hypothesis, supported by computational modelling, that some anterior follicle cells near polar cells are not exposed to high Upd concentrations because this signalling molecule is funnelled away by adjacent domains, resulting in asymmetries of STAT activation. Cells further from the polar cells may receive high Upd along adjacent, funnelling clefts, but at a later time. This is reminiscent of results in Zebrafish showing that collection of morphogen in pockets of tissue influences the responses of nearby cells<sup>47</sup>.

When too few or too many border cells are specified, migration is disrupted, suggesting that there is an optimal number of motile cells, usually between 6–8 (ref. 5). It was postulated that the cells closest to the polar cells all became motile, which would limit the number of border cells, since, on average, 6.4 follicle cells can fit around the polar cells (Table 1). Our results suggest, though, that a more complex counting mechanism must operate to ensure that a sufficient number of cells are specified: this system must be robust enough to buffer the effects of various possible distributions of the activating protein due to differences in the underlying tissue geometry. In addition, it is curious that even mutant egg chambers with large subapical extracellular domains can specify a large number of presumptive border cells. A compensatory

mechanism to upregulate Upd or STAT signalling may exist to allow sufficient signalling in this case.

Our mathematical model demonstrates that the underlying tissue on the apical side of the anterior epithelium is sufficient to alter the spatial distribution of Upd, and thereby explain the asymmetric specification of border cells. Interestingly, our model suggests that the impact of a cleft on local concentrations of signalling molecules changes with time: earlier it may act as a sink for a secreted factor, whereas later the factor is pooled along the cleft, thereby increasing its available levels for signalling to the adjacent tissue. Currently, it is difficult to observe the position of the cleft relative to the border cells and the precise size of the domain, and these may shift as the egg chamber develops. Thus, it is not surprising that we did not see exact alignment of clefts and activated cells, since Upd distribution and cell surface binding occurs hours before we examined the cell activation patterns. However, the model recapitulates the *in vivo* specification patterns over a wide range of cleft sizes and positions, and even small clefts had a detectable impact.

While the development of this model took advantage of the relatively simple tissue architecture of the *Drosophila* egg chamber, it is likely to be relevant in other contexts<sup>48</sup> and could be adapted. Little research has investigated the role of extracellular domains on the actions of diffusible signalling molecules, although several studies have considered three dimensions more generally, or how cell packing creates ‘tortuosity’ in the domains morphogens traverse<sup>1,3,47,48</sup>. Developing leg and wing imaginal discs, though, have epithelial sheets of complex topography that bound the domains in which morphogens act<sup>49,50</sup>, so this may provide a comparable situation. For tissues in which cells are very tightly packed, secreted signals must move through complex paths. In vertebrate developing limbs, the effects of signalling molecules such as retinoic acid, fibroblast growth factors (FGFs) and Sonic hedgehog are likely to be altered by how they diffuse between cells, which is considered in some models<sup>51,52</sup>. Similarly, in the mammalian brain, how tightly cells are arranged has been shown to affect the distribution of signalling molecules, even when there are only small gaps between cells<sup>53,54</sup>. Notably, recent studies demonstrate that FGF can pool in microluminal domains to concentrate its effect in Zebrafish lateral line migration<sup>47</sup>. Thus, our work strongly supports the idea that to understand how diffusible signalling molecules control cellular responses, the influence of the surrounding complex landscape must be taken into consideration, and that modelling will improve our understanding of these effects.

## Methods

**Drosophila genetics.** Fly stocks and crosses were maintained at 25 °C. Flies were incubated at 29 °C for 16 h before dissection for optimal Gal4/UAS transgene expression. The following genotypes were used: Canton S (wild type, Bloomington Stock Center); *slbo* reporter = *slbo*-Gal4 (ref. 25), UAS-mCD8-GFP/CyO (ref. 26); STAT activity reporter = 10XSTAT92E-GFP (ref. 28); UAS-*Kuz*<sup>DN</sup> (ref. 39) (Bloomington Stock Center); enhancer trap *upd*-Gal4, UAS-*Upd* 21.2 and UAS-*Upd* 26.2 (ref. 21; provided by Dr D. Montell); *apt*<sup>KG05830</sup> insertional mutant stock<sup>19,55</sup> (Bloomington Stock Center); *hfp*<sup>9</sup>, *th*, *st*, *cu*, *sr*, *e*/TM2; *hfp*<sup>13</sup>,

*st, cu, e, ca/TM2, Ubx and hfp*<sup>38</sup>, *st, cu, e, rec2/TM2* stocks<sup>43</sup> (gifts from Dr G. Schüpbach); *dome-LacZ* = *w<sup>67c23</sup> P[*lacW*]*dome<sup>G0282</sup>/FM7c** (Bloomington Stock Center).

**Immunofluorescence.** Ovary dissection and staining was performed using standard methods<sup>56</sup>. Briefly, fixation was performed using 4% formaldehyde in 0.1 M phosphate buffer (pH 7.4) for 10 min. After washing in NP40 buffer, the following primary antibodies and dilutions were used in overnight incubation: rat anti-Drosophila E-cadherin (1:25; ref. 57), mouse anti-Fasciclin III (Fas III; 1:50; ref. 58), mouse anti-Armadillo (anti-Arm; 1:40; ref. 59), mouse anti-Eya 1 (1:1,000; ref. 60), (DCAD2, Fas III 7G10, Arm N2 7A1 and Eya 10H6 antibodies from the Developmental Studies Hybridoma Bank, developed under the auspices of the NICHD, and maintained by the University of Iowa, Department of Biology, Iowa City, Iowa 52242); rat anti-Slbo (1:1,000; ref. 11), rabbit anti-STAT (1:1,000; ref. 61) and rabbit anti-APT (1:1,000; ref. 64) were gifts from Drs P. Rorth, D. Montell, and R. Schuh, respectively. For Supplementary Figs, the following additional primary antibodies and dilutions were used: chicken anti- $\beta$ -galactosidase (1:500, Aves) and rabbit anti-cleaved caspase 3 (1:400, Cell Signaling). After washes, the following secondary antibodies and dilutions were used: chicken anti-GFP (1:250; Life Sciences), Molecular probes Alexa Fluor secondary antibodies (488, 568 and 647 nm; 1:400), 4,6-diamidino-2-phenylindole (DAPI; 1:1,000; Life Sciences) was added for 10 min after secondary antibodies, then washed out. To visualize cortical actin in the nurse cells, Alexa-568-Phalloidin dye was added to egg chambers (1:50; Life Technologies) in  $1 \times$  PBS (Sigma-Aldrich) with 1% bovine serum albumin (VWR) and incubated for 25 min, followed by several washes in NP40 buffer.

**Upright imaging.** Upright imaging method is described in detail in ref. 24. Briefly, melted glycerol jelly was spread over microscope slides and chilled overnight. Stage 8 or 9 egg chambers were chosen under a Leica fluorescent stereoscope, transferred with a needle to the slides, and covered with glycerine jelly and chilled at 4 °C overnight. Columns of mounted egg chambers were cut out under a dissection scope using 45° angle miniature scalpel (Fine Science Tools) and transferred to a coverslip with anterior side of egg chambers facing down. Coverslips and blocks were mounted on slides and imaged upright. Upright images were acquired on a Leica SP5 confocal microscope equipped with Leica LAS software. Three-dimensional reconstructions of upright egg chamber optical sections were acquired using PerkinElmer Volocity 3D Image Analysis software, which allows volumetric analysis and projections of stacks of images into 2D representations. Upright imaging experiments were performed at least three times for each genotype, and data were pooled. Horizontal images were acquired on a Zeiss Axioimager Z1 microscope equipped with Axiovision software and the Apotome structural interference system (Zeiss) for optical sectioning. Adobe Photoshop CS6 was used to process and format images.

For cell counts, both 3D projections and Z-stacks of individual optical sections were analysed, both as single channels and in overlays, to identify individual cells. Optical sections were acquired from the first focal plane that displayed signal through the extent of border cell marker expression. Depth and width of clefts identified by 3D projections were measured in laterally mounted egg chambers using Leica LAS software, and using cortical actin to approximate the cell surface. Cleft depth was measured from the apical border of polar cells to the deepest part of a V created by edges of two adjacent nurse cells, in  $\mu\text{m}$ ; clefts were only considered if the V lay directly adjacent to activated cells; cleft width was measured from the apex of the nurse cell (the part closest to the follicular epithelium) to the apex of the neighbouring nurse cell. Cleft area was determined by the approximation  $1/2 \times \text{width} \times \text{depth}$ . Measurements were consistent between lateral and upright egg chambers. Upright egg chambers were analysed using Volocity Imaging Software to rotate image planes.

**Mathematical modelling.** We created a 3D representation of the extracellular domain between epithelium and nurse cells using COMSOL Multiphysics (Comsol Multiphysics 3.5a), a finite element analysis software, and used COMSOL's general form PDE module to create simulations of the time-dependent diffusion of Upd using the equations shown in the text. The domain was constructed of two contiguous components: a thin space between epithelium and nurse cells  $\Omega$  ( $(-50 \mu\text{m}, 50 \mu\text{m}) \times (-50 \mu\text{m}, 50 \mu\text{m}) \times (0 \mu\text{m}, -0.2 \mu\text{m})$ ) and a cleft between nurse cells. The cleft is either a single gap between two nurse cells ( $(-50 \mu\text{m}, 50 \mu\text{m}) \times \text{cleft width} \times \text{cleft depth}$ ) or a Y-shaped gap between three nurse cells, with one of the three branches modelled as a variable cross-section (cleft width  $\times$  cleft depth), and the other two as constant cross-sections ( $0.5 \mu\text{m} \times 0.5 \mu\text{m}$ ). Clefts were modelled as rectangular prisms, since our analyses showed that the area of the domain, not its shape, was the feature that gave rise to changes in activation.

The Upd source, via secretion from the polar cells, was positioned at the centre of the epithelial surface with uptake along the top surface, excluding the polar cells, and zero flux at the nurse cell boundaries, and imposed domain ends. We derived the essential influx of Upd ( $45 \text{ pM} \mu\text{m} \text{ s}^{-1}$ ) to elicit a concentration in the range of 4,000 pM at about the 6 h mark in line with *in vitro* experiments<sup>42</sup>. (We can also confirm that this value for sigma is reasonable by estimating a vesicular density

times vesicular release rate to yield:

$$\begin{aligned} & 5 \times 10^2 \frac{\text{molecules}}{\text{vesicle}} \times \frac{1 \text{ vesicle}}{25 \mu\text{m}^2 \cdot 12 \text{ min}} \times \frac{1 \text{ min}}{60 \text{ s}} \times \frac{1 \text{ mol}}{6.02 \times 10^{23} \text{ molecules}} \times \frac{1 \times 10^{15} \mu\text{m}}{1 \text{ L}} \\ & \approx \frac{45 \text{ pM} \mu\text{m}}{\text{s}} \end{aligned}$$

where the vesicle density of Upd, which is  $\sim 10$  times larger than insulin, would take about a factor of 1,000 fewer molecules per vesicle (ref. 62) ( $5 \times 10^5$  with a release rate reasonably lower than that of insulin ( $1 \mu\text{m}^{-2} \text{ s}^{-1}$ ; ref. 63). The maximal decay rate ( $5 \times 10^{-4} \text{ s}^{-1}$ ) in a volume given in ref. 37 is transformed into the surface uptake flux by imposing the surface to volume ratio in the thin epithelium-nurse cell space,  $0.2 \mu\text{m}$ , to get  $k = 1 \times 10^{-4} \text{ s}^{-1}$ .) The diffusion coefficient is a middling estimate from refs 41,40.

The distance between the epithelium and nurse cells in wild type was  $d = 0.2 \mu\text{m}$ , cleft geometries were constructed using blocks of variable dimension, and the depth and width of the blocks were modified using parametric sweeps. In order to imitate the top-down perspective visualized in fluorescent imaging, our solution set was graphically analysed in a volume plot with overlaid contours and a multislice grid. Each square on the grid represented an individual follicle cell, and cells that received a concentration above 3,900 pM over 50% of their surface were determined to be activated for border cell specification and motility. Colour scales for the heat maps shown in Figs 4 and 5, and Supplementary Figs 6 and 7 show middle range values to allow comparisons. We were able to compare our upright imaging views of border cell activation patterns to those predicted by the COMSOL 3D plot groups.

## References

- Wartlick, O., Kicheva, A. & Gonzalez-Gaitan, M. Morphogen gradient formation. *Cold Spring Harb. Perspect. Biol.* **1**, a001255 (2009).
- Ashe, H. L. & Briscoe, J. The interpretation of morphogen gradients. *Development* **133**, 385–394 (2006).
- Muller, P. & Schier, A. F. Extracellular movement of signaling molecules. *Dev. Cell* **21**, 145–158 (2011).
- King, R. C. *Ovarian Development in Drosophila melanogaster* (Academic Press, 1970).
- Montell, D. J., Yoon, W. H. & Starz-Gaiano, M. Group choreography: mechanisms orchestrating the collective movement of border cells. *Nat. Rev. Mol. Cell Biol.* **13**, 631–645 (2012).
- Horne-Badovinac, S. & Bilder, D. Mass transit: epithelial morphogenesis in the Drosophila egg chamber. *Dev. Dyn.* **232**, 559–574 (2005).
- Denef, N. & Schupbach, T. Patterning: JAK-STAT signalling in the Drosophila follicular epithelium. *Curr. Biol.* **13**, R388–R390 (2003).
- Dobens, L. L. & Raftery, L. A. Integration of epithelial patterning and morphogenesis in Drosophila ovarian follicle cells. *Dev. Dyn.* **218**, 80–93 (2000).
- Ghiglione, C. *et al.* The Drosophila cytokine receptor Domeless controls border cell migration and epithelial polarization during oogenesis. *Development* **129**, 5437–5447 (2002).
- Silver, D. L. & Montell, D. J. Paracrine signaling through the JAK/STAT pathway activates invasive behavior of ovarian epithelial cells in Drosophila. *Cell* **107**, 831–841 (2001).
- Beccari, S., Teixeira, L. & Rorth, P. The JAK/STAT pathway is required for border cell migration during Drosophila oogenesis. *Mech. Dev.* **111**, 115–123 (2002).
- Xi, R., McGregor, J. R. & Harrison, D. A. A gradient of JAK pathway activity patterns the anterior-posterior axis of the follicular epithelium. *Dev. Cell* **4**, 167–177 (2003).
- Montell, D. J., Rorth, P. & Spradling, A. C. Slow border cells, a locus required for a developmentally regulated cell migration during oogenesis, encodes Drosophila C/EBP. *Cell* **71**, 51–62 (1992).
- Van de Bor, V., Zimniak, G., Cerezo, D., Schaub, S. & Noselli, S. Asymmetric localisation of cytokine mRNA is essential for JAK/STAT activation during cell invasiveness. *Development* **138**, 1383–1393 (2011).
- Hombria, J. C. & Brown, S. The fertile field of Drosophila Jak/STAT signalling. *Curr. Biol.* **12**, R569–R575 (2002).
- Arbouzova, N. I. & Zeidler, M. P. JAK/STAT signalling in Drosophila: insights into conserved regulatory and cellular functions. *Development* **133**, 2605–2616 (2006).
- Zeidler, M. P. & Bausek, N. The Drosophila JAK-STAT pathway. *JAKSTAT* **2**, e25353 (2013).
- Hayashi, Y. *et al.* Glypicans regulate JAK/STAT signaling and distribution of the Unpaired morphogen. *Development* **139**, 4162–4171 (2012).
- Starz-Gaiano, M., Melani, M., Wang, X., Meinhardt, H. & Montell, D. J. Feedback inhibition of Jak/STAT signaling by apontic is required to limit an invasive cell population. *Dev. Cell* **14**, 726–738 (2008).
- Starz-Gaiano, M., Melani, M., Meinhardt, H. & Montell, D. Interpretation of the Upd/JAK/STAT morphogen gradient in Drosophila follicle cells. *Cell Cycle* **8**, 2917–2925 (2009).

21. Silver, D. L., Geisbrecht, E. R. & Montell, D. J. Requirement for JAK/STAT signaling throughout border cell migration in *Drosophila*. *Development* **132**, 3483–3492 (2005).
22. Monahan, A. J. & Starz-Gaiano, M. Socs36E attenuates STAT signaling to optimize motile cell specification in the *Drosophila* ovary. *Dev. Biol.* **379**, 152–166 (2013).
23. Lie, Y. S. & Macdonald, P. M. Apontic binds the translational repressor Bruno and is implicated in regulation of oskar mRNA translation. *Development*. **126**, 1129–1138 (1999).
24. Manning, L. & Starz-Gaiano, M. Upright imaging of *Drosophila* egg chambers. *J. Vis. Exp.* **97**, doi: 10.3791/52636 (2015).
25. Rorth, P. *et al.* Systematic gain-of-function genetics in *Drosophila*. *Development* **125**, 1049–1057 (1998).
26. Lee, T. & Luo, L. Mosaic analysis with a repressible cell marker for studies of gene function in neuronal morphogenesis. *Neuron* **22**, 451–461 (1999).
27. Belu, M. *et al.* Upright imaging of *Drosophila* embryos. *J. Vis. Exp.* doi: 10.3791/2175 (2010).
28. Bach, E. A. *et al.* GFP reporters detect the activation of the *Drosophila* JAK/STAT pathway in vivo. *Gene Expr. Patterns* **7**, 323–331 (2007).
29. Bier, E. *et al.* Searching for pattern and mutation in the *Drosophila* genome with a P-lacZ vector. *Genes Dev.* **3**, 1273–1287 (1989).
30. Andersson, E. R., Sandberg, R. & Lendahl, U. Notch signaling: simplicity in design, versatility in function. *Development* **138**, 3593–3612 (2011).
31. Bray, S. Notch signalling in *Drosophila*: three ways to use a pathway. *Semin. Cell Dev. Biol.* **9**, 591–597 (1998).
32. Grammont, M. & Irvine, K. D. fringe and Notch specify polar cell fate during *Drosophila* oogenesis. *Development* **128**, 2243–2253 (2001).
33. Vachias, C., Couderc, J. L. & Grammont, M. A two-step Notch-dependant mechanism controls the selection of the polar cell pair in *Drosophila* oogenesis. *Development* **137**, 2703–2711 (2010).
34. Assa-Kunik, E., Torres, I. L., Schejter, E. D., Johnston, D. S. & Shilo, B. Z. *Drosophila* follicle cells are patterned by multiple levels of Notch signaling and antagonism between the Notch and JAK/STAT pathways. *Development* **134**, 1161–1169 (2007).
35. Lopez-Schier, H. & Johnston, D. Delta signaling from the germ line controls the proliferation and differentiation of the somatic follicle cells during *Drosophila* oogenesis. *Genes Dev.* **15**, 1393–1405 (2001).
36. Lieber, T., Kidd, S. & Young, M. W. kuzbanian-mediated cleavage of *Drosophila* Notch. *Genes Dev.* **16**, 209–221 (2002).
37. Wang, X., Adam, J. C. & Montell, D. Spatially localized Kuzbanian required for specific activation of Notch during border cell migration. *Dev. Biol.* **301**, 532–540 (2007).
38. Prasad, M. & Montell, D. J. Cellular and molecular mechanisms of border cell migration analyzed using time-lapse live-cell imaging. *Dev. Cell* **12**, 997–1005 (2007).
39. Pan, D. & Rubin, G. M. Kuzbanian controls proteolytic processing of Notch and mediates lateral inhibition during *Drosophila* and vertebrate neurogenesis. *Cell* **90**, 271–280 (1997).
40. Zhou, S. *et al.* Free extracellular diffusion creates the Dpp morphogen gradient of the *Drosophila* wing disc. *Curr. Biol.* **22**, 668–675 (2012).
41. Kicheva, A. *et al.* Kinetics of morphogen gradient formation. *Science* **315**, 521–525 (2007).
42. Wright, V. M., Vogt, K. L., Smythe, E. & Zeidler, M. P. Differential activities of the *Drosophila* JAK/STAT pathway ligands Upd, Upd2 and Upd3. *Cell Signal.* **23**, 920–927 (2011).
43. Van Buskirk, C. & Schupbach, T. Half pint regulates alternative splice site selection in *Drosophila*. *Dev. Cell* **2**, 343–353 (2002).
44. Quinn, L. M. *et al.* *Drosophila* Hfp negatively regulates dmyc and stg to inhibit cell proliferation. *Development* **131**, 1411–1423 (2004).
45. Borensztein, A., Boissoneau, E., Fernandez, G., Agnes, F. & Pret, A. M. JAK/STAT autocontrol of ligand-producing cell number through apoptosis. *Development* **140**, 195–204 (2013).
46. McLean, P. F. & Cooley, L. Protein equilibration through somatic ring canals in *Drosophila*. *Science* **340**, 1445–1447 (2013).
47. Durdu, S. *et al.* Luminal signalling links cell communication to tissue architecture during organogenesis. *Nature* **515**, 120–124 (2014).
48. Umulis, D. M. & Othmer, H. G. The importance of geometry in mathematical models of developing systems. *Curr. Opin. Genet. Dev.* **22**, 547–552 (2012).
49. Kornberg, T. B. The imperatives of context and contour for morphogen dispersion. *Biophys. J.* **103**, 2252–2256 (2012).
50. Teلمان, A. A., Strigini, M. & Cohen, S. M. Shaping morphogen gradients. *Cell* **105**, 559–562 (2001).
51. Zhang, Y. T., Alber, M. S. & Newman, S. A. Mathematical modeling of vertebrate limb development. *Math. Biosci.* **243**, 1–17 (2013).
52. Dillon, R. & Othmer, H. G. A mathematical model for outgrowth and spatial patterning of the vertebrate limb bud. *J. Theor. Biol.* **197**, 295–330 (1999).
53. Thorne, R. G. & Nicholson, C. In vivo diffusion analysis with quantum dots and dextrans predicts the width of brain extracellular space. *Proc. Natl Acad. Sci. USA* **103**, 5567–5572 (2006).
54. Sykova, E. & Nicholson, C. Diffusion in brain extracellular space. *Physiol. Rev.* **88**, 1277–1340 (2008).
55. Bellen, H. J. *et al.* The BDGP gene disruption project: single transposon insertions associated with 40% of *Drosophila* genes. *Genetics* **167**, 761–781 (2004).
56. McDonald, J. A., Pinheiro, E. M., Kadlec, L., Schupbach, T. & Montell, D. J. Multiple EGFR ligands participate in guiding migrating border cells. *Dev. Biol.* **296**, 94–103 (2006).
57. Oda, H., Uemura, T. & Takeichi, M. Phenotypic analysis of null mutants for DE-cadherin and Armadillo in *Drosophila* ovaries reveals distinct aspects of their functions in cell adhesion and cytoskeletal organization. *Genes Cells* **2**, 29–40 (1997).
58. Patel, N. H., Snow, P. M. & Goodman, C. S. Characterization and cloning of fasciclin III: a glycoprotein expressed on a subset of neurons and axon pathways in *Drosophila*. *Cell* **48**, 975–988 (1987).
59. Riggelman, B., Schedl, P. & Wieschaus, E. Spatial expression of the *Drosophila* segment polarity gene armadillo is posttranscriptionally regulated by wingless. *Cell* **63**, 549–560 (1990).
60. Bonini, N. M., Leiserson, W. M. & Benzer, S. The eyes absent gene: genetic control of cell survival and differentiation in the developing *Drosophila* eye. *Cell* **72**, 379–395 (1993).
61. Jang, A. C., Chang, Y. C., Bai, J. & Montell, D. Border-cell migration requires integration of spatial and temporal signals by the BTB protein Abrupt. *Nat. Cell Biol.* **11**, 569–579 (2009).
62. Michael, D. J., Xiong, W., Geng, X., Drain, P. & Chow, R. H. Human insulin vesicle dynamics during pulsatile secretion. *Diabetes* **56**, 1277–1288 (2007).
63. Michael, D. J., Ritzel, R. A., Haataja, L. & Chow, R. H. Pancreatic beta-cells secrete insulin in fast- and slow-release forms. *Diabetes* **55**, 600–607 (2006).
64. Eulenberg, K. G. & Schuh, R. The tracheae defective gene encodes a bZIP protein that controls tracheal cell movement during *Drosophila* embryogenesis. *EMBO*. **16**, 7156–7165 (1997).

## Acknowledgements

We appreciate assistance from members of the fly community, particularly Dr Denise Montell, Dr Pernille Rorth and Dr Gertrud Schüpbach for reagents. We thank Flybase, the Bloomington *Drosophila* Stock Center and Developmental Studies Hybridoma Bank for information and providing fly stocks and antibodies, respectively. We acknowledge Bilal Moiz for technical assistance and Dr Jeff Leips for assistance with statistical analyses. We also thank Dr Nick Gaiano for critical comments on the manuscript and Dr Caryn Navarro for discussion of experiments. L.A.M. is supported by the Department of Education grant, Graduate Assistance in the Areas of National Need training fellowship (P200A120017) and by a National Institute of General Medical Sciences Initiative for Maximizing Student Development grant (2 R25-GM55036). A portion of the microscopy work was supported by National Science Foundation (NSF) Major Research Instrumentation grant DBI-0722569 and the Keith R. Porter Core Imaging Facility. This material is based upon work supported by the National Science Foundation under an NSF CAREER Award (1054422), and a Basil O'Connor Starter Scholar Award from the March of Dimes, both awarded to M.S.-G. Mathematical model development was funded in part by an NSF-Undergraduate Biology and Mathematics training grant (1031420).

## Author contributions

L.A.M. performed all biological experiments. L.A.M., B.E.P. and M.S.-G. conceived the biological experiments and hypotheses. A.M.W. and B.E.P. designed and implemented the mathematical modelling. L.A.M. and M.S.-G. wrote the manuscript, and all authors contributed to revisions and approved the final submitted draft.

## Additional information

**Supplementary Information** accompanies this paper at <http://www.nature.com/naturecommunications>

**Competing financial interests:** The authors declare no competing financial interests.

**Reprints and permission** information is available online at <http://npg.nature.com/reprintsandpermissions/>

**How to cite this article:** Manning, L. *et al.* Tissue landscape alters adjacent cell fates during *Drosophila* egg development. *Nat. Commun.* 6:7356 doi: 10.1038/ncomms8356 (2015).